



ITER edge database investigations of the SOL width

K. McCormick^{a,*}, N. Asakura^b, S. Bosch^a, S. Davies^c, S. Fielding^d, K. Itami^b,
H. Kawashima^b, B. LaBombard^e, B. Lipschultz^e, A. Loarte^f, R. Monk^c,
G. Porter^g, J. Schweinzer^a, M. Shimada^b, M. Sugihara^h

^a Max Planck Institut für Plasmaphysik, Boltzmannstrasse 2, 85748 Garching, Germany

^b JAERI, Naka Fusion Research Establishment, Ibaraki-ken, 311-01 Japan

^c JET Joint Undertaking, Abingdon, Oxfordshire OX14 3EA, UK

^d UKAEA Fusion, Culham Science Centre, Abingdon, Oxfordshire, OX14 3DB, UK

^e MIT Plasma Science and Fusion Center, Cambridge, MA 02139, USA

^f The NET-Team, MPI für Plasmaphysik, EURATOM Association, 85748 Garching, Germany

^g Lawrence Livermore National Laboratory, PO Box 808, Livermore, CA 94550, USA

^h ITER Joint Central Team, Joint Working Site, 85748 Garching, Germany

Abstract

Based on the ITER edge database, comparisons among the major tokamaks (ASDEX, ASDEX-Up, COMPASS-D, C-MOD, DIII-D, JET, JFT-2M and JT-60U) with respect to systematic SOL-width behavior are presented in terms of free-form regression analysis for λ_{n_e} and λ_{T_e} . Emphasis is placed on OH-L plasmas as this data is most abundant and coherent. Despite differences in size, wall-conditioning and divertor configuration, broadly similar trends are found in the regimes of low- and high-recycling and partially-detached divertor operation. In the low-recycling regime all machines appear to underlie a size scaling: $\lambda_{n_e}(\text{min}), \lambda_{T_e}(\text{min}) \sim \text{const.}(\text{surface area}/I_p)^{0.7}$. Operation at high q95, high densities with respect to the Greenwald limit, or high powers leads to SOL widths considerably in excess of the values indicated by this simple scaling, and are documented in the form of machine-specific or machine-group-specific parametric expressions. For ELMy H-modes there is a general, but not universal, trend of smaller λ_{n_e} and λ_{T_e} being associated with higher core confinement. On ASDEX-Up the SOL pressure e-folding length can vary as $n_e I_p^{-2}$ for ELMy H-modes. © 1999 Elsevier Science B.V. All rights reserved.

Keywords: ITER; Scaling law; SOL width; Tokamak

1. Introduction

The efficacy of ITER with respect to power handling and particle control depends on how well the divertor and divertor baffles have been optimized with respect to properties of the SOL, i.e. with respect to the power decay length in the divertor and to falloff lengths of the density λ_{n_e} and temperature λ_{T_e} in the SOL. Since ITER SOL performance cannot yet be reliably predicted from

theory or 2D fluid codes, parallel approaches are to attempt either an empirical extrapolation, or at least to delineate an operational region, based on the characteristics of present day tokamaks. At the same time one may hope to elucidate underlying physics via inter-machine comparisons, and to motivate further, more definitive experiments. To these ends a multi-machine SOL database has been assembled, consisting of ASDEX, ASDEX-Up (AUG), DIII-D, C-MOD, COMPASS-D, JET(Mk 0-I-II), JFT-2M and JT-60U. Of the 2137 time slices in the ITER edge database, 1128 are dedicated to SOL-width studies, of which 1/3 are H-mode. A significant fraction of these points have been discussed in the past on a machine-specific basis [1–4], as well as between machines [5–7]. This paper deals specifically with widths

* Corresponding author. Tel.: +49 89 3299 01; fax: +49 89 3299 2200; e-mail: maccormick@sat.ipp-garching.mpg.de.

of temperature and density profiles, measured in the SOL outside the divertor and flux-referenced to the outer midplane. Companion papers address the topics of separatrix density n_{es} [8] and power flux width at the target plates [9].

2. Database parameters

Whereas the ELMy H-mode is the projected mode of operation for ITER, most of the coherent data within the database is for OH-L conditions. Table 1 lists machine parameters for the OH-L scaling studies below, along with an ITER reference set. ASDEX has a circular plasma ($\kappa = 1$) with a closed double-null (DN) divertor operated sequentially with open and partially closed bypasses as well as wall conditioning by carbonization and boronization [4,10,11]. COMPASS-D, JET, JFT-2M and JT-60U have SN open divertors with ‘horizontal’ target plates, AUG and DIII-D are closed SN (horizontal plates), C-MOD is closed SN with closed bypasses [3] (vertical target plates). For the selected dataset the ion-grad-B drift direction is towards the x-point for all SN machines except JET. With the exception of COMPASS-D and JFT-2M, SOL widths associated with $P_{tot} > 1.3P_{Hth}$ (H-mode power threshold $\sim n_e^{0.69} B^{0.91} S_{area}^{0.96}$) are not considered. Further dataset restrictions for OH-L analysis are: only deuterium discharges with no impurity puffing, and no time slices where the H-factor seemed too high with respect to other points of a particular machine.

A description of the entire SOL profile in terms of an exponential falloff width does not always suffice, and the definitions of ‘width’ are not uniform within the database: ASDEX [12,13], AUG [14], and JT-60U [1] observe a steep SOL gradient near the separatrix followed by a flatter region, but it is usually possible to exponentially fit the profile beyond the 1/e point, and the value does not depend critically on the separatrix position. DIII-D uses the local gradient at the ‘separatrix’ of the Tanh fit [8] to define the SOL width. C-MOD finds a continually decreasing gradient with increasing distance from the separatrix, which is related to the local T_e [3]; here λ_{n_e} and λ_{T_e} are given as integrals out to the 1/e point and normalized such as to permit comparison with simple exponential fits. Widths so defined for C-MOD are necessarily larger than the local gradient at the separatrix, and may yield different scaling relationships than those based totally on localized quantities.

The separatrix temperature T_{es} is a leading quantity in characterizing SOL widths, and thus the exact position of the separatrix is of great importance. Within the database, four different methods are employed to define the separatrix: ASDEX, C-MOD, COMPASS-D, JFT-2M and JT-60U rely on magnetic reconstruction, sometimes code-benchmarked. Additionally, AUG cor-

rects many points by assuming classical electron heat conduction along field lines in connection with P_{sol} , λ_{T_e} and T_{es} [15]. DIII-D ‘regularizes’ the separatrix by placing it 50% of the T_e gradient length outside the Tanh symmetry point [8]. JET uses electron pressure balance along field lines between the midplane and divertor [16]. Due at least to the variety of approaches, potential uncertainties exist in making comparisons among SOL widths using n_{es} and T_{es} on a multi-machine basis. In Section 3, this aspect motivates the characterization of SOL behavior using the global parameters n_e and P_{tot} , as well as local quantities.

3. Regression analysis results for OH-L

Table 2 summarizes OH-L regression analysis for λ_{n_e} and λ_{T_e} . These are divided into two subsections, classified as ‘high-recycling’ and ‘low-recycling’, whereby high-recycling for the purposes of this paper is taken to be the region for T_{es} below the point where an increase in SOL width with $T_{es}^{-\alpha}$ just becomes apparent. (JFT-2M is assumed to be totally in the low-recycling range.) High recycling is properly defined as that regime where the particle flux to the target plate increases non-linearly with n_{es} ; however, such information is normally not available within the SOL database, making it impossible to precisely delineate high-recycling and partial detachment regimes.

Choice of regression parameters is guided by whatever global and independent local quantities are necessary to produce a satisfactory ‘free fit’ to the data. However, the choice is not unique; in an exemplary way in Table 2, different sets of parameters for the same dataset are shown to yield equally good results. Hence, T_{es} can often be replaced by n_e . The Greenwald parameter $n_{eGW} = 10^{14} I_p / \pi a_{min}^2$ [17] is introduced as a variable in the form n_e / n_{eGW} . $q95$ in combination with κ , R_{mag} or S_{area} ($\sim \kappa^{0.5} a_{min} R_{mag}$) is used, although the connection length ($\sim \kappa^{0.7} q95 R_{mag}$) does just as well on occasion (not shown). P_{tot} emerges as a more robust parameter over the database than $P_{sol} = P_{tot} - P_{rad}$. Finally, as JFT-2M has no tabulated T_{es} values, inter-machine comparisons involving JFT-2M necessarily employ global quantities.

3.1. Regression analysis: ‘high-recycling’

From classical heat conduction along open field lines one expects λ_{T_e} to vary with electron temperature as $T_{es}^{-4/5}$ [18]. A strong inverse dependence of λ_{T_e} vs. T_{es} is indeed apparent from Fig. 1a for AUG, C-MOD, JET and JT-60 for $T_{es} < 50$ –60 eV, i.e. the high-recycling regime. The JET data falls into two groups, OH and NBI-heating, making it apparent that P_{tot} as well as T_{es} will be important in arriving at a parametrical descrip-

Table 1

Parameters of ITER edge database(OH-L): a_{\min} = minor radius, R_{mag} = radius of magnetic axis, S_{area} = surface area, n_e = line density [m^{-3}], $n_{e\text{GW}}$ = Greenwald density limit, n_{es} = separatrix density, P_{tot} = total deposited power, $P_{\text{Hth}}[\text{W}]$ = H-mode power threshold = $4.1 \times 10^4 n_e [10^{20} \text{m}^{-3}]^{0.69} B_t^{0.91} S_{\text{area}}^{0.96}$, $v^* = [(\text{connection length from outer midplane to outer divertor})/(\text{e-e mean free path})]$

Machine (# points used) v^* min–mean–max	κ a_{\min} [m] R_{mag} [m] S_{area} [m^2]	B_t [T] I_p [10^6 A] q95	n_e [10^{19}m^{-3}] $n_e/n_{e\text{GW}}$ n_{es}/n_e	P_{tot} [10^6 W] $P_{\text{tot}}/P_{\text{Hth}}$
ASDEX (196)	1 0.4 1.65	1.8–2.8 0.15–0.45 2.0–8.7	0.8–5.5	0.12–1.9
0.3–2.4–13	26		0.10–1.16 0.07–0.29	
ASDEX-Up (24)	1.65 0.5 1.69	2–3 0.58–1.0 3.1–6.2	2.5–9.6 0.2–0.78	0.47–2.5 0.35–1.2
5.3–19–42	39		0.23–0.81	
C-MOD (47)	1.63 0.22 0.68	2.8–7.9 0.45–1.1 3.3–5.1	6.7–30 0.13–0.45	0.51–2.7 0.38–1.4
9–24–68	7.7		0.5–1.0	
COMPASS-D (45)	1.6 0.18 0.56	0.8–1.85 0.11–0.22 3.0–6.2	1.3–5.8 0.08–0.40	0.08–0.69 0.8–3.5
0.2–0.9–2.6	5.1		0.08–0.21	
DIID (14)	1.7–1.9 0.6 1.71	2.1 0.86–1.26 4.4–5.9	1.9–4.2 0.24–0.42	0.46–1.9 0.35–1.3
4.6–15–45	54		0.28–0.46	
JET Mk I (33)	1.74 0.9 2.96	1.5–3.4 2 2.2–4.9	2.5–5.6 0.31–0.70	1.26–5.4 0.2–1.0
4–15–34	131		0.24–0.53	
JFT-2M (8)	1.35 0.29 1.31	1.25 0.11–0.22 3.4–7	1.4–3.8 0.17–0.47	0.16–0.67 0.76–2.6
low?	18			
JT-60U (25)	1.41 0.94 3.5	2.1–4.0 1.2–1.9 3.5–6.1	1.2–4.3 0.24–0.86	3.4–4.2 0.47–1.31
2.4–12–40	145		0.14–0.48	
ITER for $n_{\text{es}} = 4 \cdot 10^{19}$ & $T_{\text{es}} = 200 \text{ eV}$ $v^* = 6$	1.6 2.8 8.14 1000	5 20 3.1		100

tion of λ_{T_e} . The high values of JT-60 are related to formation of an X-point MARFE. In Fig. 1(b), λ_{n_e} is given vs. T_{es} : λ_{n_e} is similar in behavior and magnitude for ASDEX, AUG, JET and JT-60U. Above 50 eV (low-recycling) both ASDEX and JT-60U increase with T_{es} . The lowest JT-60U points are at 2.1 T and $P_{\text{tot}}/P_{\text{Hth}} > 1$. Since they may represent borderline H-mode behavior, these points are excluded in further analysis.

High-recycling λ_{T_e} : As listed in the Table 2, AUG, JET, C-MOD (not shown) and the three machines combined yield $\lambda_{T_e} \sim T_{\text{es}}^{-\alpha}$, with α -values of 1.34 (JET) – 1.6 (C-MOD) – 2 (AUG), and 1.6 (combination), meaning that all vary faster than expected from classical parallel heat conductivity assuming an invariant $\chi_{e\perp}$. The combination scaling $\lambda_{T_e} = 0.0023 T_{\text{es}}^{-1.62} q95^{0.55} P_{\text{tot}}^{0.44} S_{\text{area}}^{0.39}$ (with a regression coefficient $R=0.96$) is plotted in

Table 2
OH-L regression fits for λ_{T_c} and λ_{n_e} for 'high'- and 'low'-recycling regimes, in the form $\lambda_{T_c} = \text{const } T_{es}^{\alpha} n_e^{\beta}$

Machine	Constant	T_{es}	n_e	n_e/n_{eGW}	q95	I_p	B_t	P_{tot}	κ	R_{mag}	S_{area}	R
λ_{T_c} high												
AUG	2.65×10^{-5}	-2.03 ± 0.65	1.36 ± 0.57					0.88 ± 0.25				0.99
JET	4.50×10^{-3}	-1.34 ± 0.13	0.39 ± 0.11					0.46 ± 0.06				0.93
AUG JET	1.48×10^{-4}	-1.59 ± 0.14	0.37 ± 0.13					0.59 ± 0.06			0.50 ± 0.07	0.95
AUG C-	2.26×10^{-3}	-1.62 ± 0.22	0.55 ± 0.23					0.44 ± 0.09			0.39 ± 0.04	0.96
MOD JET												
AUG	2.96×10^{-9}		0.37 ± 0.18					1.03 ± 0.13				0.99
ASDEX	6.85×10^{-5}	-0.37 ± 0.08	1.23 ± 0.07					0.44 ± 0.08				0.90
λ_{n_e} high												
AUG	5.88×10^{-3}	-1.23 ± 0.16						0.36 ± 0.09				0.99
ASDEX	1.40×10^{-4}			0.35 ± 0.09				0.29 ± 0.04				0.90
AUG	1.30×10^{-4}			0.57 ± 0.11				0.33 ± 0.08				0.94
JET	4.05×10^{-4}			0.42 ± 0.21				0.29 ± 0.07				0.85
ASDEX	2.40×10^{-4}			0.46 ± 0.05				0.28 ± 0.02				0.86
AUG JET												
ASDEX	1.67×10^{-12}		0.39 ± 0.0					-0.77 ± 0.13			0.66 ± 0.11	0.86
AUG JET												
λ_{T_c} low												
JFT-2M	0.013											0.97
COMPASS-	27.96											0.99
D JFT-2M								-0.38 ± 0.12			1.07 ± 0.08	
JT-60U	2.27×10^{-5}											0.80
AUG DIID	0.129		0.14 ± 0.1					-0.67 ± 0.48			1.27 ± 0.26	0.95
JET									2.3 ± 0.8			
AUG C-MOD	5.79×10^{-8}							0.69 ± 0.20			0.36 ± 0.05	0.95
DIID JET									1.27 ± 0.85			
All, no JT	42.55							0.71 ± 0.03			0.66 ± 0.03	0.95
-60U 2.1T									-1.23 ± 0.3			

λ_{ne} low	ASDEX	4.21×10^{-4}	0.27 ± 0.05	0.66 ± 0.04		0.16 ± 0.02		0.88
	JT-60U	7.07×10^{-4}	0.50 ± 0.28	0.77 ± 0.1				0.74
	JT-60U	2.41×10^{-3}	0.25 ± 0.14			0.82 ± 0.08		0.94
	COMPASS-D	1.99×10^{-4}	0.55 ± 0.14	1.26 ± 0.06		-0.45 ± 0.1		0.82
	ASDEX-	7.57×10^{-5}	0.31 ± 0.06	0.76 ± 0.06		-0.27 ± 0.07	0.14 ± 0.02	0.56 ± 0.03
	COMPASS-D							
	ASD C	4.39×10^{-4}	0.30 ± 0.06	0.75 ± 0.06		0.21 ± 0.06	0.15 ± 0.02	0.93
	JT-60U							
	$nu^* < 3.5$							
	ASDEX	0.774	–	0.58 ± 0.05		0.10 ± 0.07	0.28 ± 0.02	0.89
	COMPASS-D	2238	–	0.76 ± 0.1				0.8
	JFT-2M	0.007		0.77 ± 0.1				0.96
	JT-60U	0.006				0.85 ± 0.1		0.89
	ASDEX JT	7.74	–	0.46 ± 0.05		0.33 ± 0.06	0.26 ± 0.02	-1.4 ± 0.07
	-60U							0.87
	ASD	0.2	–	0.63 ± 0.05		-0.11 ± 0.06	0.21 ± 0.17	0.92
	COMPASS							
	JFT-2M							
	AUG C-	6.03×10^{-12}	0.39 ± 0.2	0.89 ± 0.27		-0.89 ± 0.25	0.22 ± 0.17	1.04 ± 0.25
	MOD							0.94
	DIII D JET							
	All except	90.92		0.15 ± 0.07		-0.61 ± 0.05	0.24 ± 0.03	0.56 ± 0.11
	JT-60U							1.13 ± 0.08
	All except	1.04		0.11 ± 0.06		-0.72 ± 0.04	0.22 ± 0.03	0.11 ± 0.09
	JT-60U							0.69 ± 0.02
								0.90

^a The exponents with error bars are located in the column headed by the regression parameter. Blank spaces indicate the regression parameter was either not important or not used due to co-linearities. Abbreviations: ASD = ASDEX, JET = JET(MkI), C = COMPASS-D. *All, no JT-60U 2.1T* = all OH-L points in the database are used with exception of those from JT-60U at 2.1 T.

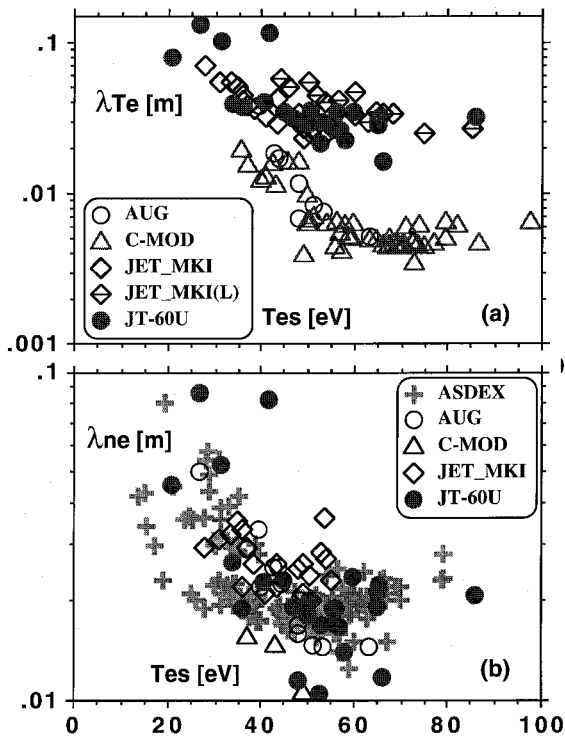


Fig. 1. λ_{Te} (a) and λ_{ne} (b) vs. T_{es} . (a) λ_{Te} not available for ASDEX. (b) For clarity only OH values given for ASDEX and JET; L-mode points lie mostly $T_{es} > 50$ eV with $\lambda_{ne} \sim 3$ –6 cm. Most C-MOD points lie below 1 cm: $\lambda_{ne}(B_t > 3T)$ is the same as λ_{Te} ; $\lambda_{ne}(B_t < 3T) \sim 2$ –3 mm.

Fig. 2a. Introduction of I_p as a variable leads to a better organization of points for C-MOD while maintaining the ordering for AUG and JET: $\lambda_{Te} = 35.3 T_{es}^{-1.65} q95^{0.5} I_p^{-0.97} P_{tot}^{0.65} S_{area}^{0.67}$, $R = 0.96$ (not shown in table). However, there is co-linearity between size and I_p (AUG = 1 MA, C-MOD = 0.5–1 MA, JET = 2 MA), and between P_{tot} and I_p on C-MOD (only OH discharges remain after selection process), rendering the indicated I_p dependence questionable. Nevertheless, assuming $T_{es} = 200$ eV, ITER predictions of the two expressions are $\lambda_{Te} \sim 3.6$ and 1.5 cm, respectively. For AUG, λ_{Te} can also be brought into connection with the Greenwald limit: $\lambda_{Te} \sim (n_e/n_{eGW})^{0.37} q95^{1.2} P_{tot}^{1.0}$, i.e. with similar exponents for q95 and P_{tot} – implying the approach to the Greenwald limit as $(n_e/n_{eGW})^{0.37}$ is equivalent to $T_{es}^{-2.0}$.

High-recycling λ_{ne} : As extant in Fig. 1(b) and Table 2, λ_{ne} increases with decreasing T_{es} more slowly for ASDEX than either AUG or JET. It is likely that ASDEX, having a lower-recycling divertor, does not penetrate as rapidly into the high recycling regime as a function of T_{es} . Nonetheless, large λ_{ne} for ASDEX still emerge, partly because of higher q95 values (up

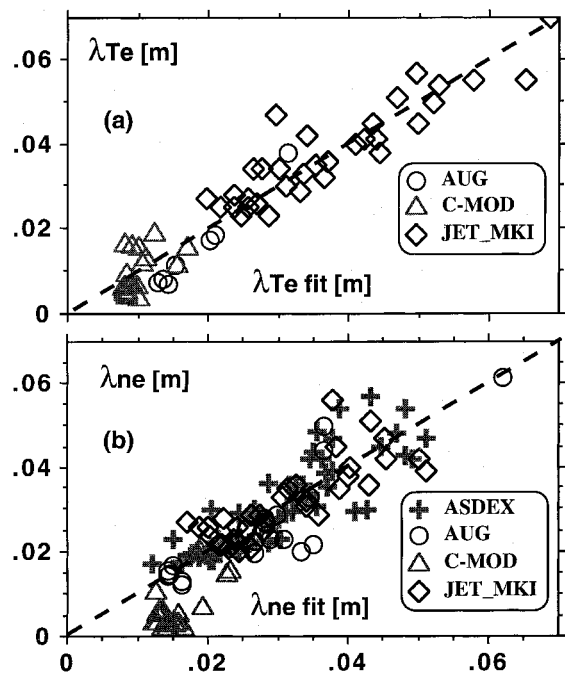


Fig. 2. High-recycling: (a) $\lambda_{Te,fit} = 0.0023 T_{es}^{-1.62} P_{tot}^{0.44} q95^{0.55} S_{area}^{0.39}$, (b) $\lambda_{ne,fit} = 2.4 \times 10^{-4} (n_e/n_{eGW})^{0.46} P_{tot}^{0.28} q95^{1.13} B_t^{-0.30}$. C-MOD values not used in λ_{ne} regression.

to 8.7). These machines can also be characterized using n_e/n_{eGW} . The combined scaling is: $\lambda_{ne} \sim (n_e/n_{eGW})^{0.46} q95^{1.13} P_{tot}^{0.28} B_t^{-0.3}$, illustrated in Fig. 2(b). An interesting aspect is any size scaling appears to be adequately contained within $n_{eGW} \sim I_p/\pi a_{min}^2$. Using n_e and the parameters κ and R instead of n_{eGW} yields: $\lambda_{ne} \sim n_e^{0.39} q95^{1.56} P_{tot}^{0.30} B_t^{-0.77} R_{mag}^{0.66}$. The form is globally the same in terms of n_e , I_p , B_t and P_{tot} , only now B_t explicitly appears more strongly. Keeping in mind the moderate quality of the fit in Fig. 2(b) (and assuming $n_e/n_{eGW} = 0.6$), λ_{ne} (ITER) ~ 0.07 m.

3.2. Regression analysis: ‘low-recycling’

Low recycling is loosely defined as being that where $T_{es} > 40$ –50 eV pertains. All of the data from COMPASS-D, and JFT-2M (it is assumed) lie here, a considerable part from ASDEX and JT-60, and only vestiges from AUG, C-MOD, DIII-D, and JET.

Low-recycling λ_{Te} : Referring to Table 2, λ_{Te} for JFT-2M can be described as $\lambda_{Te} \sim q95^{0.76}$. JFT-2M and COMPASS-D together yield: $\lambda_{Te} \sim n_e^{-0.2} q95^{0.68} P_{tot}^{0.10} B_t^{-0.38} R_{mag}^{1.07}$, which is also approximately the result for COMPASS-D alone using these parameters (not shown). Of interest is the negative density exponent, i.e. λ_{Te} decreases with increasing n_e , just the opposite of that observed in the high recycling regime. The combinations

AUG, DIII-D and JET, and then including C-MOD, are well represented ($R=0.95$). But, these fits must be regarded with suspicion, as the changes in parametrical dependencies are radical in going from one group to the other: the I_p exponent alters from -0.6 to 0.7 and S_{area} from 1.27 to 0.36 . Finally, combining all machines leads to: $\lambda_{Te} = 42.6\kappa^{-1.23}S_{\text{area}}^{0.66}I_p^{-0.71}$ (ITER prediction = 0.015 m), shown in Fig. 3a. C-MOD, COMPASS-D, DIII-D, JFT-2M and JT-60U are reasonably compatible with the fit. JET lies above the curve – perhaps understandably, as even these low-recycling points are in the rollover regime (i.e., where the target plate particle flux no longer increases with n_{es}) [2]. However, there is no apparent reason for the AUG values being a factor of two too low.

Low-recycling λ_{n_e} : The next six lines of Table 2 analyze λ_{n_e} for ASDEX, COMPASS-D, JT-60U, and combinations thereof in terms of T_{es} . λ_{n_e} for ASDEX and JT-60U increase moderately with T_{es} [2,11]. The exponent of T_{es} for JT-60U changes from 0.5 to 0.25 when B_t is substituted for $q95$ – which also produces a better fit ($R=0.74$ vs. 0.94). COMPASS-D has a T_{es} exponent of 0.55 (also positive), with field dependence of $B_t^{-0.45}$. However, introducing the separatrix density n_{es} as a parameter leads to $\lambda_{n_e} \sim T_{\text{es}}^{0.31}q95^{0.77}n_{\text{es}}^{-0.24}$, $R=0.85$, (not shown), i.e. the explicit B_t dependence vanishes. Removing T_{es} from the regression leads to a best fit [5]: $\lambda_{n_e} \sim q95^{0.45}B_t^{0.22}n_{\text{es}}^{-0.43}P_{\text{tot}}^{0.12}$, $R=0.86$ (not shown), i.e. with a positive B_t exponent. Evidently, the interdependencies among n_{es} , T_{es} and B_t lead to superficially contradictory results contingent on the chosen combination.

The grouping ASDEX/COMPASS-D, and then with JT-60U added, reproduces the scaling for ASDEX alone, with a weak $B_t^{-0.21}$ factor originating from COMPASS-D. The size scaling necessary to bring the first group into cohesion is $S_{\text{area}}^{0.56}$, but adding JT-60 leads to the replacement of $S_{\text{area}}^{0.56}$ with $\kappa^{-1.9}$.

For purposes of contrast and in order to facilitate comparisons with JFT-2M, analysis is continued using n_e instead of T_{es} . λ_{n_e} (ASDEX) $\sim q95^{0.6}n_e^{-0.18}B_t^{0.1}P_{\text{tot}}^{0.3}$. Combining COMPASS-D and JFT-2M yields $\lambda_{n_e} \sim q95^{0.72}n_e^{-0.26}R_{\text{mag}}^{0.66}$, $R=0.95$ (not shown), about the same as for COMPASS-D alone. This size scaling is maintained: $\lambda_{n_e} \sim R_{\text{mag}}^{0.64}$ for ASDEX/COMPASS-D/JFT-2M.

Again, the set AUG/C-MOD/DIII-D/JET can be ordered nicely for λ_{n_e} , with the same reservations as for λ_{Te} . The combination $q95^{0.89}B_t^{-0.89}$ indicates I_p is the relevant parameter (since $q95 \sim B_t/I_p$). The entire dataset, excluding JT-60, can be expressed as $\lambda_{n_e} = 90.9n_e^{-0.103}q95^{0.15}I_p^{-0.61}P_{\text{tot}}^{0.24}\kappa^{0.56}R_{\text{mag}}^{1.13}$, or replacing R_{mag} with S_{area} : $\lambda_{n_e} = 1.04q95^{0.11}I_p^{-0.72}P_{\text{tot}}^{0.22}\kappa^{0.11}S_{\text{area}}^{0.69}$ (Fig. 3(b)). For ITER (at $n_e/n_{\text{es}} = 0.6$) both predict $\lambda_{n_e} \sim 0.04$ m. Note, as with λ_{Te} the factor $(S_{\text{area}}/I_p)^{0.7}$ stands out as an important quantity. In Fig. 4 the entire OH-L database is plotted vs. $10.5(S_{\text{area}}/I_p)^{0.7}$, the 10.5 being the factor necessary to define a line just underneath all points. This expression reliably delineates, except for C-MOD, a minimum λ_{n_e} -scaling for all machines. Thus high current densities are synonymous with small SOL widths, with the actual experiment widths depending on all the factors elucidated in Table 2.

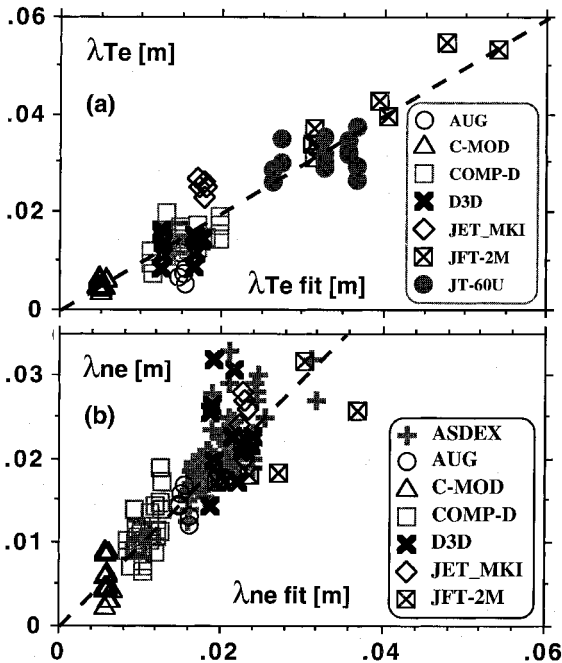


Fig. 3. Low-recycling: (a) $\lambda_{Te, \text{fit}} = 42.5I_p^{-0.71}S_{\text{area}}^{0.66}\kappa^{-1.2}$, JT-60U (2.1 T) excluded; (b) $\lambda_{Te, \text{fit}} = 1.04P_{\text{tot}}^{0.22}q95^{0.11}I_p^{-0.72}S_{\text{area}}^{0.69}\kappa^{0.11}$.

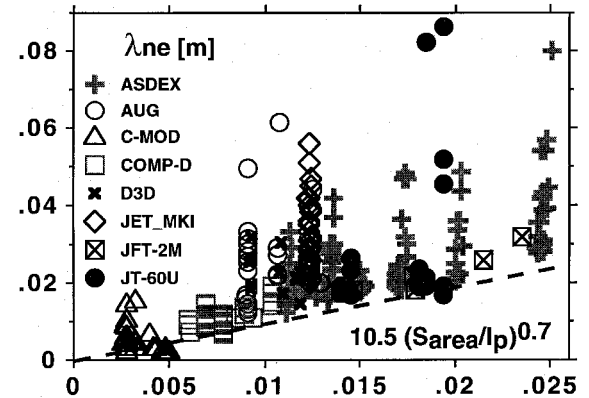


Fig. 4. λ_{n_e} vs. $10.5(S_{\text{area}}/I_p)^{0.7}$. All OH-L points, excepting JT-60U at 2.1 T, are plotted. This expression describes the lower boundary of each machine, whereas the vertical spread is described by the machine-specific expressions of Table 2.

4. Regression analysis H-mode

There are 360 time slices with an H-mode label in the SOL database: AUG (118), C-MOD(20), DIII-D (209), JET MkI (2), JET MkII (7) and JFT-2M (4). Of these, only a subset of the AUG data (46) contains a parameter scan in I_p and n_e with a meaningful regression. DIII-D is unique in that λ_{n_e} (8.6 ± 3.6 mm) and λ_{T_e} (5.2 ± 1.5 mm) do not appear to underlie any systematic trends. There are too few points for JFT-2M: λ_{n_e} (12.7 ± 1.9 mm) and λ_{T_e} (no values). Nonetheless, many machines do share common qualitative tendencies: With impurity- or increasing gas-puffing, the SOL becomes broader and confinement decreases, i.e. the best confinement and shortest SOL falloff lengths generally occur for discharges with no external neutral fuelling beyond that provided by the neutral beam heating. On JET this behavior is clearly associated with an increase in ELM frequency ν_{ELM} and a change from type I to type III ELMs [19], whereby the SOL widths exhibit a direct correlation with ν_{ELM} and puff rate [20].

Restricting the AUG H-mode dataset to discharges with no impurity puffing, D_2 gas puffing $< 10^{22}/s$ and 2.5 T, the electron pressure e-folding length varies as: $\lambda_{pe} = 9.28 \cdot 10^{-9} n_e^{1.03 \pm 0.13} I_p^{-1.96 \pm 0.2} (P_{tot} - P_{rad})^{-0.4 \pm 0.07}$ (Fig. 5). P_{tot} alone works as well as $P_{tot} - P_{rad}$; however, $P_{sol} = P_{tot} - P_{rad,core}$ is a poor fitting parameter. Here, the pressure width is addressed as it is known the pressure gradient on closed field lines, from the pedestal outwards, often comes close to a critical gradient which scales as I_p^2 [21]. The result is consistent with an extension of this gradient into the SOL. To be complete: $\lambda_{T_e} = 3.5 \cdot 10^{-6} n_e^{0.92 \pm 0.18} I_p^{-1.79 \pm 0.27} (P_{tot} - P_{rad})^{-0.63 \pm 0.09}$, $R = 0.79$ and $\lambda_{n_e} = 1 \times 10^{-10} n_e^{1.11 \pm 0.13} I_p^{-2.25 \pm 0.16}$, $R = 0.9$. The absolute numbers are: λ_{n_e} [13.5–22.4–39.2 mm] and λ_{T_e} [5.4–10.5–19.2 mm)] [min–mean–max].

On C-MOD: λ_{n_e} [1–2.9–8.4 mm] and λ_{T_e} [2–6.8–18 mm]); one finds: $\lambda_{n_e} = 1.61 \cdot 10^{10} T_{es}^{-1.49 \pm 0.35} P_{tot}^{-1.62 \pm 0.67}$,

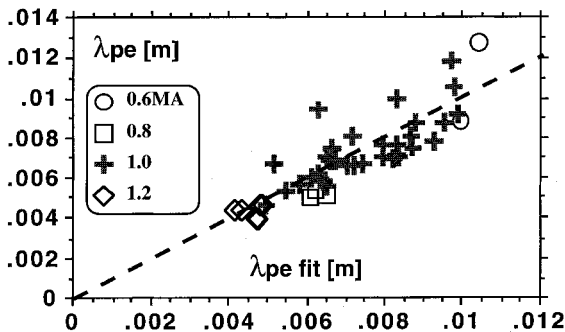


Fig. 5. λ_{pe} fit = $9.3 \times 10^{-9} n_e^{1.0} I_p^{-2.0} (P_{tot} - P_{rad})^{-0.4}$. AUG ELMy H-mode scaling for: 2.5 T, no impurity puffing, D_2 gas puff $< 10^{22}/s$.

$R = 0.91$. Interestingly, the smallest SOL widths occur for cases where $P_{sol}/P_{tot} < 0.4$ and $P_{rad}/P_{tot} \sim 100\%$. For JET (MkII), due to D_2 - and impurity-puffing the following ranges result: λ_{n_e} [4.2–17.4–38 mm] and λ_{T_e} [5–21–32 mm].

5. Discussion

Within the OH-L dataset it transpires that for machines with high recycling divertors both λ_{n_e} and λ_{T_e} increase as $\lambda_{T_e}^{-1(1.23-2)}$ (for $T_{es} < 50-60$ eV usually). From classical heat conduction along open field lines one expects $\lambda_{T_e} \sim T_{es}^{-0.8}$. The magnitude of the exponent in excess of 0.8 can potentially be interpreted as $\chi_{e\perp} \sim T_{es}^{-\alpha}$ – as has been done in the past on the basis of local analysis within the SOL [3,22]. Also, 2D fluid code analysis of the JET divertor plasma for hot-ion H-modes dictates an increase in $\chi_{e\perp}$ moving away from the separatrix (falling T_e) in order to match the T_e profiles [23]. On the other hand, a concomitant augmentation of λ_{n_e} is not expected per se as T_{es} decreases. Naturally, for a highly-recycling divertor λ_{n_e} may be strongly influenced by local ionization sources, leading to larger λ_{n_e} . But, B2/EIRENE code calculations for ASDEX under conditions of low T_{es} did not predict any enhancement of λ_{n_e} [4], leaving room for speculation that $D_{\perp} \sim T_{es}^{-\alpha}$ ($T_{es} < 40-50$ eV) on ASDEX [24]. Finally, all machines exhibit a positive dependence on P_{tot} regardless of regime, which might indicate an enhancement in perpendicular transport with P_{tot} . Classically one expects $\lambda_{T_e} \sim P_{tot}^{-4/9}$ [18].

For low recycling, most machines demonstrate $\lambda_{n_e} \sim T_{es}^{0.25-0.5}$ or $n_e^{-(0.1-0.3)}$, (i.e. positive and negative exponents) just the opposite of high recycling. On ASDEX such behavior was shown to be consistent with perpendicular transport via ExB-driven turbulent flux [25]. Other suggestions have been advanced for COMPASS-D [5–7].

Clear trends exist in the ratio $\lambda_{n_e}/\lambda_{T_e}$ over the range high T_{es} –low T_{es} . The ratio remains constant for open-divertor machines: COMPASS (0.78 ± 0.16), JFT-2M (0.52 ± 0.05) and JT-60U (0.61 ± 0.08). Otherwise: AUG ($2.15 \pm 0.5 > 0.8$) C-MOD ($1.02 \pm 0.42 > 0.2-0.5$), JET(OH: $1- > 0.5$; NBI: $2- > 0.6$), i.e. the latter machines tend to $\lambda_{n_e}/\lambda_{T_e} \sim 0.5$ at the lowest T_{es} .

The implied B_t scalings in Table 2 depend strongly on the choice of regression parameters. COMPASS-D is a case in point (Section 3.2), where B_t appears either with a negative or positive exponent, or not at all, depending on use of T_{es} , n_{es} or both within the Ansatz. Using T_{es} and n_{es} to describe λ_{pe} on C-MOD, B_t needs not be invoked explicitly [3]. ASDEX has also reported a lack of B_t influence in the low-recycling range for λ_{n_e} when using T_{es} and q_{95} as regression parameters [11,24]. However, $T_{es}(\text{OH}) \sim B_t^{0.4}$ for ASDEX [4], and a weak B_t

dependence is present when n_e is selected as a fit parameter rather than T_{es} , as seen in Table 2.

The question of size scaling to ITER is critical, but no universal rule has materialized. Presumably, the κ -exponents of Table 2 are not significant, since (excluding ASDEX) κ varies less than 30%. The exponents for R_{mag} and S_{area} are positive: $R_{mag}^{0.6-1.1}$ or $S_{area}^{0.4-0.7}$. The most convincing all-machine scalings are in the low-recycling regime where $(S_{area}/I_p)^{0.7}$ emerges as the dominate factor. This leads to predicted minimum (OH-L) SOL widths as: $\lambda_{n_e}(\min) \sim 10.5(S_{area}/I_p)^{0.7} \sim 1$ cm (ITER) and $\lambda_{T_e}(\min) \sim 15(S_{area}/I_p)^{0.7} \sim 1.5$ cm. λ can be much larger, depending on q95, proximity to n_{eGW} or high P_{tot} (example, see Fig. 4).

In closing we note the free-form analysis of this paper is of pragmatic use in identifying principle variables and global trends. Perhaps more physics insight is attainable by directly comparing (relative) model predictions against the database [5–7,26]. At least problems of colinearities are avoided. An indication of probable difficulties inherent in absolute scalings is the experience that closing the divertor bypass on C-MOD reduced λ_{p_e} by about 40% at low T_{es} without changing the relative behavior [3]. Finally, note that DIII-D has not entered into the high-recycling analysis, as the data does not appear to underlie any system, in contrast to dedicated SOL experiments of the past [27].

6. Summary

Based on the ITER edge database, comparisons among all major tokamaks with respect to systematic SOL-width behavior have been effected in terms of regression analysis for λ_{n_e} and λ_{T_e} . Phenomenologically, the analysis is divided into two OH-L regimes: high-recycling ($T_{es} < 40$ –60 eV) where widths increase rapidly with decreasing T_{es} (ASDEX, AUG, C-MOD, DIII-D, JET, JT-60U) and low-recycling where variations are more subtle (ASDEX, COMPASS-D, JFT-2M, JT-60U). For high recycling one finds $\lambda_{T_e} \sim T_{es}^{-(1.3-2)}$ $q95^{(0.6-1.4)} P_{tot}^{(0.5-0.9)}$, or alternatively, $\lambda_{T_e} \sim (n_e/n_{eGW})^{0.4-0.6} q95^{(0.4-1.2)} P_{tot}^{0.3}$.

For low-recycling the ordering is roughly $\lambda_{T_e} \sim (S_{area}/I_p)^{0.7}$ and $\lambda_{n_e} \sim (S_{area}/I_p)^{0.7} q95^{0.11} P_{tot}^{0.22}$. ASDEX, COMPASS-D and JT-60U exhibit a relationship $\lambda_{n_e} \sim T_{es}^{0.3}$ (i.e. positive exponent) in contrast to the high recycling regime. The baseline behavior for all machines is reasonably described as: $\lambda_{T_e}(\min) \sim 15(S_{area}/I_p)^{0.7}$ and $\lambda_{n_e}(\min) \sim 10.5(S_{area}/I_p)^{0.7}$. The emergence of S_{area}/I_p as a size-scaling factor intimates a link to the quantity $I_p/(\pi a_{min}^2)$, i.e. the largest SOL widths are associated with the smallest Greenwald limits. For ITER(OH-L) the predictions are: $\lambda_{n_e}(\min) \sim 1$ cm and $\lambda_{T_e}(\min) \sim 1.5$ cm. Larger values will attain for higher q95, P_{tot} , or approach of n_e to the GW limit, as discussed above.

The modus operandi of ITER – the ELMy H-mode – cannot be adequately addressed within the existing dataset. It is broadly true the highest confinement and smallest SOL-widths are achieved with ‘natural NBI fuelling’, i.e. with no gas puffing. Attempts to augment n_e by puffing often lead to higher ELM frequencies, reduced confinement and larger SOL widths. DIII-D is an exception, where the SOL seems impervious to change, regardless of conditions. For AUG the pressure e-folding length can vary as $\lambda_{p_e} \sim n_e I_p^{-2}$. Such behavior mirrors that expected for edge pressure gradients (on closed field lines) limited by ideal ballooning modes.

This study succeeds in illuminating trends. However, it also underlines the necessity of additional dedicated experiments if inter-machine physics understanding and believable extrapolation to larger experiments is to be properly served. Specifically, coherent SOL data for ELMy H-modes is particularly dearth.

Acknowledgements

The authors acknowledge fruitful discussions with members of the ITER Expert Groups ‘Divertor Modeling’ and ‘Divertor Physics’, as well as assistance by the IPP Computer Science Department and the computer supporting staff of ITER Garching JWS. Sincere thanks also go to the team members of ASDEX, ASDEX-Up, COMPASS-D, C-MOD, DIII-D, JET, JFT-2M and JT-60U who contributed to the ITER edge database.

References

- [1] N. Asakura et al., J. Nucl. Mater. 241–243 (1997) 559.
- [2] S.J. Davies et al., Proc. 22nd EPS Conf., vol. 19C, Bournemouth, 1995, p. III-257.
- [3] B. Labombard et al., J. Nucl. Mater. 241–243 (1997) 149.
- [4] K. McCormick et al., Proc. 20th EPS Conf., vol. 17c, Lisbon, 1993, p. II-587.
- [5] J.W. Connor, UKAEA Fusion Report FUS 396, March 1998.
- [6] G.F. Counsell et al., Proc. 24th EPS Conf., vol. 21A, Berchtesgaden, 1997, p. I-253.
- [7] G.F. Counsell et al., these Proceedings.
- [8] G. Porter et al., these Proceedings.
- [9] A. Loarte et al., these Proceedings.
- [10] K. McCormick et al., J. Nucl. Mater. 176&177 (1990) 89.
- [11] K. McCormick et al., J. Nucl. Mater. 196–198 (1992) 264.
- [12] K. McCormick et al., J. Nucl. Mater. 145–147 (1987) 215.
- [13] K. McCormick et al., J. Nucl. Mater. 162–164 (1989) 264.
- [14] J. Schweinzer et al., Proc. 23rd EPS Conf. vol. 20C, Kiev, 1996, p. II-719.
- [15] J. Schweinzer et al., Proc. 24th EPS Conf., vol. 21A, Berchtesgaden, 1997, p. IV-1449.
- [16] A. Loarte et al., Nuclear Fusion 38 (1998) 331.
- [17] M. Greenwald et al., Nuclear Fusion 28 (1988) 2199.

- [18] M. Keilhacker et al., *Physica Scripta T2/2* (1982) 443.
- [19] G. Saibene et al., *Proc. 24th EPS Conf. vol. 21A*, Berchtesgaden, 1997, p. I-49.
- [20] S.J. Davies et al., these Proceedings.
- [21] W. Suttrop et al., these Proceedings.
- [22] S.K. Erents et al., *Proc. 24th EPS Conf. vol. 21A*, Berchtesgaden, 1997, p. I-121.
- [23] K. McCormick et al., *J. Nucl. Mater.* 241–243 (1997) 444.
- [24] K. McCormick et al., *Proc. 19th EPS Conf. vol. 16c*, Innsbruck, 1992, p. II-763.
- [25] M. Endler et al., *Nuclear Fusion* 35 (1995) 1307.
- [26] S.-I. Itoh, K. Itoh, *Plasma Phys. Contr. Fusion* 36 (1994) 1845.
- [27] J.G. Watkins et al., *J. Nucl. Mater.* 196–198 (1992) 829.